# Linking the basement geology along the Africa-South America coasts in the South Atlantic

**Jiří Konopásek[1,2], Jiří Sláma[3,4] and Jan Košler[3,*]**

[1]*Department of Geosciences, University of Tromsø – The Arctic University of Norway, Dramsveien 201, 9037, Tromsø, Norway*

[2]*Czech Geological Survey, Klárov 3, 118 21, Praha 1, Czech Republic*

[3]*Department of Earth Science, University of Bergen, Allégaten 41, 5007, Bergen, Norway*

[4]*Institute of Geology AS CR, v.v.i., Rozvojová 269, 165 00 Praha 6, Czech Republic*

[*] *deceased*

_____

**ABSTRACT**

The match of geological units of the dissected Kaoko-Dom Feliciano-Gariep orogenic system exposed along the coasts of the South Atlantic is poorly understood. Two suites of intrusive rocks crop out in the Angra Fria Bay area, a part of the Coastal Terrane of the Kaoko Belt in Namibia. U–Pb zircon dating of three samples from the younger suite provided ages of $574 \pm 6$, $586 \pm 3$ and $584 \pm 7$ Ma, similar to the ages of the oldest syn-collisional granitoids in the area. Three samples of the older suite gave ages of $626 \pm 5$, $622 \pm 5$ and $620 \pm 6$ Ma respectively, which have not previously been recorded in intrusive rocks of the Kaoko Belt, but which coincide with those from the Florianópolis Batholith in the Dom Feliciano Belt in Brazil. Zircon ages, Sr–Nd isotopic composition and tectonic position of these granitoids suggest that this magmatic complex could be a continuation of the Florianópolis Batholith on the African side of the Atlantic Ocean. Consequently, the Angra Fria intrusions and the Florianópolis Batholith may represent suitable localities for spatial reconstruction of the Gondwana supercontinent in the area, where the robust pre-Mesozoic connecting points are scarce.

**Keywords:** Gondwana reconstruction, South Atlantic Ocean, plate tectonics, Kaoko Belt, Dom Feliciano Belt.

**1. Introduction**

Arguably the oldest remark about the connection of American continents with Africa and Europe was made by a Dutch geographer Abraham Ortelius in his Thesaurus Geographicus (Ortelius, 1596), where he writes (freely translated from Latin): "…Gadir as a part of Atlantis or of the Island of America, were not submersed … but were torn away from

_____

Europe and Africa by earthquakes and floods." … "The vestiges of the rupture reveal themselves, if someone brings forward a map of the World and considers carefully the coasts of these three lands where they face each other: it is evident that the promontory of Europe and of course Africa, fit the concavity of the Americas."

A serious discussion of the link between Europe, Africa and the American continents started c. 100 year ago. The matching shape of the Atlantic coastlines, the even better fit of the continental shelves and the similarities in paleontological records were mentioned when Wegener (1912) formulated the continental drift theory. More than 50 years later, Bullard et al. (1965) and Smith and Hallam (1970) provided the first quantification of the fit along the edges of the Atlantic continental shelves. Since then, ongoing discussion of a rigorous fit of South America and Africa is based mainly on studies of syn-rifting or post-break-up features, such as the continent-ocean boundaries, prominent fracture zones, salt basins and syn-rifting deposits along the Atlantic coasts (e.g. Le Pichon and Hayes, 1971; Sibuet and Mascle, 1978; Rabinowitz and LaBrecque, 1979; Martin et al., 1981; Vink, 1982; Unternehr et al., 1988; Nürnberg and Müller, 1991; Eagles, 2007; Torsvik et al., 2009; Moulin et al., 2010; Blaich et al., 2011; Heine et al., 2013).

The fit of pre-Mesozoic geological features along the shores on both sides of the South Atlantic Ocean remains poorly understood. A major challenge in any correlation of the pre-rifting geological units are the usually >150 km wide shelves and the syn- to post-rifting onshore deposits, which both obscure a substantial part of the pre-Mesozoic geological record. De Wit et al. (2008) compiled a list of well-dated steep tectonic features that can serve as matching points for the pre-rifting geological record-based re-assembly of Africa and South America. However, the shorelines of Uruguay, southeastern Brazil and Namibia cut the pre-Mesozoic coastal tectonic units at low angles, which, in combination with the wide shelves, may cause a large lateral offset of the corresponding geological units in the map (Fig.

_____

1). Therefore, the connection of pre-rifting geological features is apparently easier in the area

of the Gulf of Guinea and its counterpart in Brazil than in the southern parts of both

continents (de Wit et al., 2008).

Porada (1979) discussed the similarities in the evolution of the geological units

presently called the Dom Feliciano, Kaoko and Gariep belts (Fig. 1) providing the first

correlation between the pre-Mesozoic geology of southeastern Brazil/Uruguay and Namibia.

Nevertheless, the exact spatial link of the units exposed along the coasts of Namibia,

southeastern Brazil and Uruguay is poorly understood and the evidence of their matching

Neoproterozoic evolution is only based on similar timing of tectonic processes (Basei et al.,

2005; Gross et al., 2009; Oyhantçabal et al., 2009; Lenz et al., 2011). We add new evidence

for a simultaneous late Neoproterozoic magmatic activity in the northern parts of the Kaoko

and Dom Feliciano belts. Laser ablation–inductively coupled plasma–mass spectrometry

(LA–ICP–MS) and secondary ion mass spectrometry (SIMS) zircon U–Pb dating and isotopic

analysis of magmatic rocks cropping out at the Angra Fria Bay in northwestern Namibia

reveal the so far unrecognized character of these intrusions in the context of the Kaoko Belt

evolution and provide argumentation for their temporally and spatially robust correlation with

the magmatic rocks of the northernmost Dom Feliciano Belt. All directions used below refer

to the present-day configuration.


**2. Geological context**

The Kaoko Belt is part of a N–S trending Neoproterozoic orogenic system involving

also the Gariep Belt in SW Namibia and the Dom Feliciano Belt in SE Brazil and Uruguay

(Fig. 1; e.g. Porada, 1979; Basei et al., 2000; Frimmel et al., 2011). The Kaoko Belt consists

of two major tectonic units represented by the margin of the Congo Craton with its

sedimentary cover, and the overriding Coastal Terrane (Fig. 1). Both units collided at *ca.*

_____

580–550 Ma (Goscombe and Gray, 2008). The Congo Craton margin is dominated by the

Archean–Mesoproterozoic basement underlying the metamorphosed Neoproterozoic

sedimentary cover (Seth et al., 1998; Kröner et al., 2004) represented by clastic sediments and

carbonates deposited between >740 Ma and *ca.* 580 Ma in two distinct cycles with contrasting

sources of the detrital material (Konopásek et al., 2014). The metamorphic grade increases

from east to west reaching partial melting conditions along the contact with the Coastal

Terrane (Goscombe et al., 2003). The Coastal Terrane consists of metamorphosed sediments

and presumably syn-sedimentary volcanic rocks dated at *ca.* 800 Ma (Konopásek et al.,

2008). Metamorphism of the Coastal Terrane reached partial melting conditions at *ca.* 650–

630 Ma, i.e. about 80–100 Ma earlier than in the underlying deformed cratonic margin, which

experienced its metamorphic peak at *ca.* 550 Ma (Franz et al., 1999). The migmatization of

the Coastal Terrane was connected with limited magmatism at *ca.* 650 Ma, whereas the 580–

550 Ma thrusting over the Congo Craton margin was accompanied by intrusion of

voluminous plutons into the Coastal Terrane rocks (Seth et al., 1998; Kröner et al., 2004;

Konopásek et al., 2008; Janoušek et al., 2010).

Gross et al. (2009), Oyhantçabal et al. (2009) and Lenz et al. (2011) correlated the

Coastal Terrane with the Punta del Este Terrane in the Dom Feliciano Belt (Fig. 1). This

correlation is based on the common presence of *ca.* 800–770 Ma igneous rocks

metamorphosed in the granulite facies at *ca.* 650–630 Ma, a combination of features unique to

the Dom Feliciano-Kaoko-Gariep orogenic system. The Punta del Este Terrane crops out to

the east of a pre-Neoproterozoic crustal domain extending between the Rio de la Plata Craton

and the Luis Alves Terrane (Fig. 1) representing the western foreland of the Kaoko-Dom

Feliciano-Gariep orogenic system (e.g. Basei et al., 2000). Along the contact of the western

foreland with the Punta del Este Terrane there is a suite of granitoid rocks called the Granite

Belt, which is subdivided into the Aiguá, Pelotas and Florianópolis batholiths (Fig. 1). The

_____

timing of these intrusions between *ca.* 630–570 Ma is coeval with the magmatic activity

recorded in the foreland unit west to northwest of the Granite Belt (Babinski et al., 1997;

Leite et al., 1998; Remus et al., 1999; 2000; Koester et al., 2001; da Silva et al., 1999; 2005;

Hartmann et al., 2002; Gaucher et al., 2008; Oyhantçabal et al., 2009; Passarelli et al., 2010;

Basei et al., 2011; Chemale et al., 2012; Florisbal et al., 2012a; Martini et al., 2015).


## 3. The Angra Fria Magmatic Complex

The Angra Fria Magmatic Complex (AFMC) is part of the Coastal Terrane of the

Kaoko Belt and crops out in the area of the Angra Fria Bay (Fig. 1). Detailed mapping (Fig.

2) has revealed that the AFMC consists of two suites of plutonic rocks (Fig. 3a) that intrude a

migmatitic gneiss complex. The older suite of variably deformed porphyritic granites (Fig.

3b) and diorites is accompanied by small intrusions of undeformed coarse-grained hornblende

gabbros (Fig. 3c). The younger suite is represented by hornblende granodiorite–tonalite body,

coarse-grained, weakly porphyritic biotite granite, medium-grained muscovite-biotite granite

with weak magmatic or no fabric and a dioritic dyke crosscutting the gneiss complex (Fig.

3d). The country rocks are clinopyroxene-bearing gneisses, amphibolites and felsic

migmatitic gneisses. The map presented in Fig. 2 covers the area with the best accessibility

and much larger extent of the complex, especially along the coast towards the north, cannot

be ruled out.

Whole rock powders and zircons extracted from three samples of the older (NJ-57,

NJ-58 and NJ-59) and three samples of the younger suite (NJ-62, NK-42 and NJ-05) were

used for U–Pb, Sr–Nd and Hf isotopic analysis. Detailed description of analytical methods is

provided in the appendix A and the results of the LA–ICP–MS and SIMS U–Pb zircon dating

of the samples and Hf isotopic analysis are provided as supplementary data. Nd and Sr

_____

isotopic ratios were recalculated to their initial values (i) based on the zircon U–Pb ages and the results are provided in Tab. 1. All data are quoted with $2\sigma$ uncertainties.

### 3.1. Sample NJ-57

Sample NJ-57 (S18.23880°, E12.02201°, all coordinates are in WGS 84) is a granitic augen orthogneiss (Fig. 3b) consisting of K-feldspar, plagioclase, quartz, biotite and accessory muscovite, titanite, apatite, zircon, opaque mineral and small amount of secondary chlorite. All felsic minerals show signs of solid-state recrystallization. Cathodoluminescence (CL) imaging of the extracted zircons reveals oscillatory zoning with rare featureless cores. Some of the grains show disturbance of the oscillatory zoning along their margins. The LA–ICP–MS isotopic analysis of the oscillatory-zoned parts yielded a concordia (Ludwig, 1998) U–Pb age of $626 \pm 5$ Ma (Fig. 4a) interpreted as the crystallization age of the granitic protolith of the orthogneiss, and a mean $\varepsilon Hf_{(i)}$ of -4.9 $\pm$ 0.5. The whole-rock isotopic analysis yielded $^{87}Sr/^{86}Sr_{(i)}$ of $0.70771 \pm 0.00001$ and $\varepsilon Nd_{(i)}$ of -4.7 $\pm$ 0.1 (Tab. 1 and Fig. 5).

### 3.2. Sample NJ-59

Sample NJ-59 (S18.23999°, E12.02862°) is a diorite with the mineralogy plagioclase, amphibole, biotite, subordinate quartz and accessory titanite, opaque mineral, apatite and zircon. The sample shows weak sub-solidus deformation concentrated into the quartz aggregates. Zircons from this sample are oscillatory zoned in CL and some contain CL-darker, but still oscillatory-zoned cores. The LA–ICP–MS isotopic analysis of the zircon yielded a concordia U–Pb age of $620 \pm 6$ Ma (Fig. 4b) interpreted as the crystallization age of the diorite, and a mean $\varepsilon Hf_{(i)}$ of -4.8 $\pm$ 0.5. The whole-rock isotopic analysis provided $^{87}Sr/^{86}Sr_{(i)}$ of $0.70784 \pm 0.00001$ and $\varepsilon Nd_{(i)}$ of -4.4 $\pm$ 0.1 (Tab. 1 and Fig. 5).

_____

*3.3. Sample NJ-58*

Sample NJ-58 (S18.23851°, E12.02676°) is a coarse-grained hornblende gabbro (Fig.

3c) with the same mineralogy as the sample NJ-59. Zircons from this gabbro are either

oscillatory zoned, or show large featureless cores in CL. When analysed by LA–ICP–MS,

both zircon types yielded similar isotopic data that combine into a concordia U–Pb age of 622

± 5 Ma (Fig. 4c) and a mean $\varepsilon Hf_{(i)}$ of -2.8 ± 0.3. SIMS analysis provided isotopic data that

combine into a slightly younger concordia U–Pb age of 617 ± 4 Ma (Fig. 6a). The LA–ICP–

MS and SIMS ages overlap within their respective errors and are interpreted as the

crystallization age of the gabbro. The whole-rock isotopic analysis yielded $^{87}Sr/^{86}Sr_{(i)}$ of

0.70698 ± 0.00001 and $\varepsilon Nd_{(i)}$ of -4.0 ± 0.1 (Tab. 1 and Fig. 5).


*3.4. Sample NJ-05*

Sample NJ-05 (S18.31481°, E12.08529°) represents dioritic dyke crosscutting the

migmatitic country rocks of the AFMC (Fig. 3d). The diorite has the mineralogy plagioclase,

amphibole, biotite, subordinate quartz and opaque mineral, and accessory apatite and zircon.

Zircons from this diorite show non-concentric oscillatory zoning in CL. LA–ICP–MS isotopic

data from these zircons combine into a concordia U–Pb age of 584 ± 7 Ma (Fig. 4d)

interpreted as the time of emplacement of the dyke. Mean $\varepsilon Hf_{(i)}$ value of the zircons is -7.7 ±

0.3. The whole rock isotopic analysis provided $^{87}Sr/^{86}Sr_{(i)}$ of 0.71175 ± 0.00001 and $\varepsilon Nd_{(i)}$ of -

8.4 ± 0.1 (Tab. 1 and Fig. 5).


*3.5. Sample NK-42*

Sample NK-42 (S18.31180°, E12.09936°) represents the granodiorite–tonalite body of the

younger suite. The rock consists of plagioclase, quartz, K-feldspar, biotite, amphibole with

accessory titanite, epidote, apatite and zircon. CL images of extracted zircons show concentric

_____

oscillatory zoning and no xenocrystic cores. Isotopic dating of the zircon by SIMS provided a

concordia U–Pb age of 586 ± 4 Ma (Fig. 6b) interpreted as the crystallization age of the

sample.  The whole rock isotopic analysis provided $^{87}Sr/^{86}Sr_{(i)}$ of 0.71268 ± 0.00001 and

$\varepsilon Nd_{(i)}$ of -6.8 ± 0.1 (Tab. 1 and Fig. 5).

*3.6. Sample NJ-62*

The sample of muscovite-biotite granite NJ-62 (S18.20823°, E11.98121°) consists of

K-feldspar, plagioclase, quartz, subordinate muscovite, biotite, chlorite and accessory opaque

mineral and zircon. CL imaging of the zircons revealed the presence of xenocrystic cores

surrounded by oscillatory-zoned rims. The analysis of the oscillatory-zoned parts provided a

mean $\varepsilon Hf_{(i)}$ value of -0.6 ± 0.5. The LA–ICP–MS U–Pb dating of the oscillatory-zoned parts

yielded a cluster of ages between *ca.* 560 and 595 Ma (Fig. 4e). A group of the most

concordant data combines into a concordia age of 574 ± 6 Ma. When the data with apparent

Pb loss are considered, the resulting upper intercept gives a statistically undistinguishable age

of 575 ± 6 Ma (Fig. 4f). We interpret these ages as the best estimate of the age of the granite

crystallization. Analysis of xenocrystic cores yielded one discordant date close to c. 1250 Ma

and a scatter of dates between c. 800 Ma and the inferred crystallization age of c. 575 Ma

(Fig. 4e). The whole rock isotopic analysis provided $^{87}Sr/^{86}Sr_{(i)}$ of 0.71045 ± 0.00001 and

$\varepsilon Nd_{(i)}$ of -3.9 ± 0.1 (Tab. 1 and Fig. 5).

**4. Discussion**

*4.1. Correlation of the AFMC rocks with other granitoid rocks of the Kaoko and Dom*

*Feliciano belts*

_____

The crystallization ages of 626 ± 5, 622 ± 5 and 620 ± 6 Ma from the older suite of the AFMC are unique in the geology of the Coastal Terrane and do not overlap with the age of any magmatic rock so far dated in this unit. The intrusions associated with the migmatization of the Coastal Terrane rocks are *ca.* 25–30 Ma older (*ca.* 650 Ma) and the early syn-collisional intrusions associated with the thrusting of the of the Coastal Terrane over the Congo Craton margin are *ca.* 40–55 Ma younger, i.e. *ca.* 580–570 Ma (Fig. 7; e.g. Seth et al., 1998; Konopásek et al., 2008). The ages of these syn-collisional intrusions suggest an origin coeval with the granitoid rocks of the younger AFMC suite dated in this work at 574 ± 6, 586 ± 3 and 584 ± 7 Ma (Fig. 7).

Spatial position of the Angra Fria Magmatic Complex suggests that its intrusive rocks could link with the intrusions of the Florianópolis, Pelotas and Aiguá batholiths of the Dom Feliciano Belt (Fig. 1). The zircon ages of the older AFMC suite overlap within their respective errors with zircon ages of 625 ± 6 − 609 ± 16 Ma known for some intrusions in the Florianópolis Batholith (Fig. 1), as well as those intruding the foreland exposed to the north of that batholith (Passarelli et al., 2010; Basei et al., 2011; Chemale et al., 2012; Florisbal et al., 2012a; Martini et al., 2015). These authors also reported ages of 602 ± 4 − 587 ± 9 Ma for syn- to post-kinematic granitoids in that region, which are apparently older than the younger AFMC suite dated here, but the youngest granitoids overlap within error with samples NJ-05 and NK-42 dated in this study (Fig. 7). The oldest magmatic rocks from the Pelotas Batholith (Fig. 1) with ages of 613 ± 6 and 609 ± 17 Ma (Babinski et al., 1997; da Silva et al., 1999) are apparently younger than those for the older suite in the AFMC, but they also overlap within analytical uncertainties. Ages for some of the younger granitoids in the Pelotas Batholith dated by Babinski et al. (1997) and Koester et al. (2001) at 600 ± 10 − 594 ± 5 Ma are apparently older than the younger AFMC suite. The granitoids that intruded the foreland off the Pelotas batholith show ages between 583 ± 11 and 550 ± 6 Ma (Leite et al., 1998; Remus

_____

et al., 1999; 2000). Intrusions forming the Aiguá Batholith (Fig. 1) were emplaced between 587 ± 16 and 564 ± 7 Ma, but there are also two intrusions dated at 633 ± 8 and 627 ± 23 Ma that intruded the foreland to the west (Fig. 7; Hartmann et al., 2002; Gaucher et al., 2008; Oyhantçabal et al., 2009). The comparison above suggests a match of zircon ages of the older AFMC suite with the *ca.* 618–626 Ma old intrusions in the Florianópolis Batholith (Fig. 7)

The link between the AFMC rocks and granitoids of the Florianópolis Batholith is further supported by a good correlation of their Sr–Nd isotopic data (Fig. 5). This similarity contrasts with isotopic composition of granitoids of similar age but intruding the foreland immediately northwest of the Florianópolis Batholith, which show considerably more negative $\varepsilon Nd_{(i)}$ values (Fig. 5; Florisbal et al., 2012b,c; Chemale et al., 2012). On the other hand, comparison of the Hf isotopic data with those presented by Chemale et al. (2012) is not that straightforward. The $\varepsilon Hf_{(i)}$ values calculated for the zircons from the AFMC granitoids are between -0.6 and -7.7, whereas Chemale et al. (2012) reported mostly more negative values and also their much larger span between -4.6 and -14.6.


*4.2. Correlation of the tectonic position of the AFMC rocks with the granitoids of the Florianópolis Batholith*


Crucial for linking the AFMC rocks with the granitoids along the Dom Feliciano belt of South America is not only their age and similarity in Sr–Nd isotopic data, but also their position within the tectonic and metamorphic structure of the Kaoko and Dom Feliciano belts. The Punta del Este and Coastal terranes show similarity in protolith ages of the oldest meta-igneous rocks (i.e. *ca.* 800–770 Ma), as well as in the timing of peak metamorphism (*ca.* 650–630 Ma) and metamorphic grade. These two terranes are considered as one tectonic domain in the structure of the Dom Feliciano-Kaoko-Gariep belt system (Gross et al., 2009; Oyhantçabal

_____

et al., 2009; Lenz et al., 2011). According to this interpretation, the position of the AFMC in the westernmost exposed part of the Coastal Terrane agrees with the tectonic position of the Granite Belt that flanks the western limit of the Punta del Este Terrane (Fig. 1). As mentioned above, the Sr–Nd isotopic signatures of the AFMC granitoids correlate well with the values known for the rocks of the Florianópolis Batholith suggesting that both originated by melting of similar sources.

*4.3. Link between tectonic units and prominent structures of the Kaoko-Dom Feliciano-Gariep orogenic system*

The genetic relationship between the AFMC and the Florianópolis Batholith is further supported by their position in the tectonic maps of Africa and South America, respectively, aligned so that they show their relative position shortly before the break-up (Fig. 1; based on the work of Heine et al., 2013). This and other reconstructions quoted in the introductory chapter are based on syn- to post-rifting geological features that are independent of the position of the pre-Mesozoic geological units and thus provide an argumentation for a robust spatial link between the AFMC and the Florianópolis Batholith. On the other hand, the present-day extent of the continental shelves and syn- to post-rifting deposits along the coasts of the South Atlantic does not allow an assessment of the role of potential submerged or covered transcurrent shear zones. As the overall sense of movement along major sear zones in the Kaoko and Dom Feliciano belts is sinistral (e.g. Goscombe and Gray, 2008; Oyhantçabal et al., 2011), the transcurrent movements could have placed the Angra Fria Magmatic Complex against the Florianópolis Batholith after the emplacement of the complex somewhere farther south in the belt. However, the actual existence and extent of such translation is difficult to assess.

_____

The spatial link between the Coastal and Punta del Este terranes is not obvious (Fig. 1). Da Silva et al. (1999) and Koester et al. (2016) have reported the presence of gneisses enclosed within the granitoids of the central and northern Pelotas Batholith. These xenoliths have protolith ages and geochemical features corresponding to the rocks dated by Lenz et al. (2011) in the Punta del Este Terrane in Uruguay. Such findings indicate similar country rocks during the emplacement of the Aiguá and Pelotas batholiths and suggest a continuation of the Punta del Este Terrane farther to the north.  This fact, together with the strong similarity in temporal and metamorphic evolution of the Coastal and Punta del Este terranes mentioned by Gross et al. (2009), Oyhantçabal et al. (2009) and Lenz et al. (2011), suggests that these terranes may form a coherent unit present along the entire axis of the Kaoko-Dom Feliciano-Gariep orogenic system with the central part hidden in the shelves and underneath the post-Mesozoic deposits.

 De Wit et al. (2008) have connected the southern tip of the system of transcurrent shear zones in the Kaoko Belt (the Village and Three Palm shear zones; Goscombe and Gray, 2008) with the northern tip of the shear zone system separating the Florianópolis Batholith from the foreland units (the Sierra Ballena-Dorsal Canguçu-Major Gercino shear zone system; e.g. Basei et al., 2000) in the northern Dom Feliciano Belt (Fig. 1). However, the spatial reconstruction presented in Fig. 1 shows that these shear zones cannot be linked together due to their large lateral offset. The position within the tectonic zoning of the Kaoko-Dom Feliciano-Gariep orogenic system suggests that the Sierra Ballena-Dorsal Canguçu-Major Gercino shear zone bounds the central part of the orogen with respect to the western foreland in southern Brazil and Uruguay, whereas the Village and Three Palm shear zone system bounds it towards the eastern foreland in northern Namibia.


**5. Conclusions**

_____

The crystallization ages and Sr–Nd isotopic signatures of the older AFMC suite correlate with those known from the early syn-kinematic granitoids of the Florianópolis Batholith. The identical position of the AFMC and the Granite Belt of the Dom Feliciano Belt west of the granulitic Coastal and Punta del Este terranes, respectively, further supports the interpretation that the AFMC represents a continuation of the Granite Belt on the African side of the Atlantic Ocean. This suggests that the AFMC and the Florianópolis Batholith represent suitable localities for the spatial reconstruction of the Gondwana supercontinent in the area of the South Atlantic Ocean, where robust pre-rifting matching points are scarce.

**Appendix A. – Analytical methods**

*LA–ICP–MS zircon U–Pb dating*

The samples (*ca.* 3 kg each) were crushed and sieved, and zircon was separated using the Wilfley shaking table and heavy liquids in the laboratories of the Bergen University, Norway. Zircon grains were mounted in epoxy-filled blocks and polished for subsequent cathodoluminescence (CL) imaging. A Nu AttoM high resolution ICP-MS coupled to a 193

_____

nm ArF excimer laser (Resonetics RESOlution M-50 LR) at Bergen University, Norway, was used to measure the Pb/U and Pb isotopic ratios in zircons. The laser was fired at a repetition rate of 5 Hz and energy of 80 mJ with 19 microns spot size. Typical acquisitions consisted of 15 second measurement of blank followed by measurement of U and Pb signals from the ablated zircon for another 30 seconds. The data were acquired in time resolved – peak jumping – pulse counting mode with 1 point measured per peak for masses $^{204}$Pb + Hg, $^{206}$Pb, $^{207}$Pb, $^{208}$Pb, $^{232}$Th, $^{235}$U, and $^{238}$U. Due to a non-linear transition between the counting and attenuated (= analog) acquisition modes of the ICP instruments, the raw data were pre-processed using a purpose-made Excel macro. As a result, the intensities of $^{238}$U are left unchanged if measured in a counting mode and recalculated from $^{235}$U intensities if the $^{238}$U was acquired in an attenuated mode. Data reduction was then carried out off-line using the Iolite data reduction package version 3.0 with VizualAge utility (Petrus and Kamber, 2012). Full details of the data reduction methodology can be found in Paton et al. (2010). The data reduction included correction for gas blank, laser-induced elemental fractionation of Pb and U and instrument mass bias. For the data presented here, blank intensities and instrumental bias were interpolated using an automatic spline function while down-hole inter-element fractionation was corrected using an exponential function. No common Pb correction was applied to the data but the low concentrations of common Pb was controlled by observing $^{206}$Pb/$^{204}$Pb ratio during measurements. Residual elemental fractionation and instrumental mass bias were corrected by normalization to the natural zircon reference material GJ-1 (Jackson et al., 2004). The excess variance (Paton et al., 2010) of GJ-1 was automatically calculated in the Isoplot program (Ludwig, 2012; version 4.15) and quadratically added to the measurement uncertainties of all unknowns including validation zircon reference materials Plešovice (Sláma et al., 2008) and 91500 (Wiedenbeck et al., 1995). These two were periodically analysed during the measurement for quality control and the obtained mean

_____

values of 335.2 ± 2.2 (2σ) Ma and 1073.8 ± 5.8 (2σ) Ma are ca 0.75% accurate within the

published reference values (337 Ma, Sláma et al., 2008; 1065 Ma, Wiedenbeck et al., 1995,

respectively). The zircon U–Pb ages are presented as concordia diagrams generated with

Isoplot. Concordia ages of individual samples are pooled data with quadratic addition of the

excess variance of the primary zircon reference material GJ-1. This error propagation should

account for the artificial reduction of the age uncertainty during calculation of Concordia age

in Isoplot.


*SIMS zircon U–Pb dating*

Prior to the SIMS analysis, the samples were coated with c. 30 nm of gold and

analysed for isotopes of U, Pb and interfering molecules on a Cameca IMS 1280 ion probe at

the Swedish Museum of Natural History in Stockholm (Nordsim facility). The instrument

parameters, analytical method, calibration and correction procedures were similar to those

described by Whitehouse et al. (1999) and Whitehouse and Kamber (2005). The instrument

was operated in automated mode with 18 μm ion beam diameter. The measured Pb/U ratios

were calibrated against the reference zircon 91500, which has an age of 1065.4 ± 0.3 Ma and

U and Pb concentrations of 80 and 15 ppm, respectively (Wiedenbeck et al., 1995). Common

lead corrections assumed a modern-day average terrestrial common Pb composition

(Stacey and Kramers, 1975).


*LA–MC–ICP–MS zircon Hf isotopic analysis*

Hf isotopic measurements were carried out using a 193 nm ArF excimer laser

(Resonetics RESOlution M-50 LR) attached to a NU Plasma 2 MC ICP–MS. The laser was

fired at a repetition rate of 8 Hz and energy of 80 mJ with 47 or 64 microns spot size

depending on the available area of analyzed zircon surface. The analyzed spots were placed

_____

right next to the U–Pb laser pits to ensure that both analyses sampled the same part of the

zircon. Data for gas blank were acquired for 20s followed by 40s of laser ablation. The

faraday cup configuration was set to enable detection of all Hf isotopes as well as potentially

interfering ions: $^{171}Yb$, $^{173}Yb$, $^{174}Yb$, $^{175}Lu$, $^{176}Hf(+Lu+Yb)$, $^{177}Hf$, $^{178}Hf$, $^{179}Hf$, $^{180}Hf$. Data

reduction was carried out off-line using the Iolite data reduction package version 2.5 . Full

details of the data reduction methodology can be found in (Paton et al., 2011). Data were

corrected for gas blank and isobaric interferences of Yb and Lu on $^{176}Hf$ using $^{176}Yb/^{173}Yb =$

0.79618 (Chu et al., 2002) and $^{176}Lu/^{175}Lu = 0.02655$ (Vervoort et al., 2004). A value for

$^{179}Hf/^{177}Hf = 0.7325$ (Patchett and Tatsumoto, 1980) and the exponential law were used for

mass bias correction of interfering Yb and Lu isotopes and isotopes of Hf. The zircon

reference material Plešovice (Sláma et al., 2008) was used for normalization of the resulting

$^{176}Hf/^{177}Hf$ ratios. During the sequence, the zircon reference material 91500 (Wiedenbeck et

al., 1995) was periodically measured for quality control purpose and the average value of

$^{176}Hf/^{177}Hf = 0.282311 \pm 0.000013$ (2σ) is in good  agreement with the published value of

$0.282303 \pm 21$ (Wu et al., 2006). εHf is defined as parts per 10 000 deviation from the

chondritic composition. CHUR: $^{176}Lu/^{177}Hf = 0.0332$, $^{176}Hf/^{177}Hf = 0.282772$ (Blichert-Toft

and Albarède, 1997); $^{176}Lu$ decay constant $= 1.8648*10^{-11}$ (Scherer et al., 2001).


*Whole rock Sr–Nd isotopic analysis*

For the radiogenic isotope determinations, samples were dissolved using a combined

HF–HCl–HNO$_3$ acid attack. The isotopes were isolated by exchange chromatography

techniques following standard chemical separation described by Le Roex and Lanyon (1998).

Rb–Sr and Sm–Nd Isotopic analyses were performed on a Finnigan MAT 262 thermal

ionization mass spectrometer housed at the University of Bergen in dynamic ($^{143}Nd/^{144}Nd$ and

$^{87}Sr/^{86}Sr$) and static ($^{84}Sr/^{86}Sr$, $^{87}Rb/^{85}Rb$, $^{148}Nd/^{144}Nd$ and $^{149}Sm/^{152}Sm$) mode using a double

_____

Re filament assembly. In the case of Sr, a minor amount of $H_3PO_4$ was added to suppress

ionisation to achieve stable signals. Concentrations of Sr, Rb, Nd and Sm were quantified by

isotopic dilution with in-house $^{84}$Sr-$^{87}$Rb and $^{148}$Nd-$^{149}$Sm mixed spikes. The $^{143}$Nd/$^{144}$Nd

ratios were corrected for mass fractionation to $^{146}$Nd/$^{144}$Nd = 0.7219 (Wasserburg et al.,

1981). External reproducibility was estimated from repeat analyses of the La Jolla

($^{143}$Nd/$^{144}$Nd = 0.511850 ± 0.000006, 2σ) and NIST SRM 987 ($^{87}$Sr/$^{86}$Sr = 0.71024 ± 0.00002,

2σ) isotopic standards. Decay constants for $^{87}$Rb and $^{147}$Sm of 1.42 x $10^{-11}$ and 6.54 x $10^{-12}$,

respectively, were used (Steiger and Jaeger, 1977; Lugmair and Marti, 1978). Calculation of

Nd model ages and εNd$_{(i)}$ values are based on $^{143}$Nd/$^{144}$Nd = 0.512638 and $^{147}$Sm/$^{144}$Nd =

0.1967 for the chondritic uniform reservoir (CHUR, Jacobsen and Wasserburg, 1980) and

$^{143}$Nd/$^{144}$Nd = 0.513114 and $^{147}$Sm/$^{144}$Nd = 0.222 for depleted mantle composition (Michard et

al., 1985).


**Appendix B. (Electronic) – Supplementary data**

Tab–data_LA–ICP–MS_dating

Tab–data_LA–MC–ICP–MS_Hf


**REFERENCES**

Babinski, M., Chemale Jr., F., van Schmus, W.S., Hartmann, L.A., da Silva, L.C., 1997. U–Pb

and Sm–Nd geochronology of the Neoproterozoic granitic-gneissic Dom Feliciano Belt,

southern Brazil. J. South Am. Earth Sci. 10, 263–274.

Basei, M.A.S., Campos Neto, M.C., Castro, N.A., Nutman, A.P., Wemmer, K., Yamamoto,

M.T., Hueck, M., Osako, L., Siga, O., Passarelli, C.R., 2011. Tectonic evolution of the

_____

Brusque Group, Dom Feliciano belt, Santa Catarina, Southern Brazil. J. South Am. Earth

Sci. 32, 324–350.

Basei, M.A.S., Frimmel, H.E., Nutman, A.P., Preciozzi, F., Jacob, J., 2005. A connection

between the Neoproterozoic Dom Feliciano (Brazil/Uruguay) and Gariep (Namibia/South

Africa) orogenic belts – evidence from a reconnaissance provenance study. Precambrian

Res. 139, 195–221.

Basei, M.A.S., Siga Jr., O., Masquelin, H., Harara, O.M., Reis Neto, J.M., Preciozzi, F., 2000.

The Dom Feliciano Belt (Brazil–Uruguay) and its foreland (Rio de la Plata Craton):

Framework, tectonic evolution and correlations with similar terranes of southwestern

Africa. In: Cordani, U.G., Milani, E.J., Thomaz Filho, A., Campos, D.A. (Eds.), Tectonic

Evolution of South America. Rio de Janeiro, 311–334.

Blaich, O.A., Faleide, J.I., Tsikalas, F., 2011. Crustal breakup and continent-ocean transition

at South Atlantic conjugate margins: J. Geophys. Res. 116, B01402.

Blichert-Toft, J., Albarède, F., 1997. The Lu-Hf isotope geochemistry of chondrites and the

evolution of the mantle-crust system: Earth Planet. Sci. Lett. 148, 243–258.

Bullard, E., Everett, J.E., Smith, A.G., 1965. The Fit of the continents around the Atlantic.

Phil. Trans. Royal Soc. A 258, 41–51.

Chemale Jr., F., Mallmann, G., Bitencourt, M.F., Kawashita, K., 2012. Time constraints on

magmatism along the Major Gercino Shear Zone, southern Brazil: Implications for West

Gongwana reconstruction. Gondwana Res. 22, 184–199.

Chu, N.C., Taylor, R.N., Chavagnac, V., Nesbitt, R.W., Boella, R.M., Milton, J.A., German,

C.R., Bayon, G., Burton, K., 2002. Hf isotope ratio analysis using multi-collector

inductively coupled plasma mass spectrometry: An evaluation of isobaric interference

corrections. J. Anal. Atom. Spect. 17, 1567–1574.

_____

da Silva, L.C., Hartmann, L.A., McNaughton, N.J., Fletcher, I.R., 1999. SHRIMP U/Pb
    zircon dating of Neoproterozoic granitic magmatism and collision in the Pelotas
    Batholith, southernmost Brazil. Int. Geol. Rev. 41, 531–551.

da Silva, L.C., McNaughton, N.J., Fletcher, I.R., 2005. SHRIMP U–Pb zircon geochronology
    of Neoproterozoic crustal granitoids (Southern Brazil): A case for discrimination of
    emplacement and inherited ages. Lithos 82, 503–525.

de Wit, M.J., Stankiewicz, J., Reeves, C., 2008. Restoring Pan-African-Brasiliano
    connections: more Gondwana control, less Trans-Atlantic corruption. In: Pankhurst, R.J.,
    Trouw, R.A.J., de Brito Neves, B.B., de Wit, M.J. (Eds.), West Gondwana: Pre-Cenozoic
    correlations across the south Atlantic region. Geol. Soc. London Spec. Pub. 294, 399–
    412.

Eagles, G., 2007. New angles on South Atlantic opening. Geophys. J. Int. 168, 353–361.

Florisbal, L.M., Bitencourt, M.F., Janasi, V.A., Nardi, L.V.S., Heaman, L.M., 2012c.
    Petrogenesis of syntectonic granites emplaced at the transition from thrusting to
    transcurrent tectonics in post-collisional setting: Whole-rock and Sr–Nd–Pb isotope
    geochemistry in the Neoproterozoic Quatro Ilhas and Mariscal granites, Southern Brazil.
    Lithos 153, 53–71.

Florisbal, L.M., Janasi, V.A., Bitencourt, M.F., Heaman, L.M., 2012a. Space-time relation of
    post-collisional granitic magmatism in Santa Catarina, southern Brazil: U–Pb LA-MC-
    ICP-MS zircon geochronology of coeval mafic-felsic magmatism related to the Major
    Gercino Shear Zone. Precambrian Res. 216–219, 132–151.

Florisbal, L.M., Janasi, V.A., Bitencourt, M.F., Nardi, L.V.S., Heaman, L.M., 2012b
    Contrasted crustal sources as defined by whole-rock and Sr–Nd–Pb isotope geochemistry
    of Neoproterozoic early post-collisional granitic magmatism within the Southern
    Brazilian Shear Belt, Camboriú, Brazil. J. South Am. Earth Sci. 39, 24–43.

_____

Franz, L., Romer, R.L., Dingeldey, D.P., 1999. Diachronous Pan-African granulite-facies

metamorphism (650 Ma and 550 Ma) in the Kaoko belt, NW Namibia. Eur. J. Mineral.

11, 167–180.

Frimmel, H.E., Basei, M.S., Gaucher, C., 2011. Neoproterozoic geodynamic evolution of

SW-Gondwana: a southern African perspective. Int. J. Earth Sci. 100, 323–354.

Gaucher, C., Finney, S.C., Poiré, D.G., Valencia, V.A., Grove, M., Blanco, G.,

Pamoukaghlián, K., Peral, L.G., 2008. Detrital zircon ages of Neoproterozoic

sedimentary successions in Uruguay and Argentina: Insights into the geological evolution

of the Río de la Plata Craton. Precambrian Res. 167, 150–170.

Goscombe, B., Gray, D.R., 2008. Structure and strain variation at mid-crustal levels in a

transpressional orogen: A review of Kaoko Belt structure and the character of West

Gondwana amalgamation and dispersal. Gondwana Res. 13, 45–85.

Goscombe, B., Hand, M., Gray, D., Mawby, J., 2003. The metamorphic architecture of a

transpressional orogeny: the Kaoko Belt, Namibia. J. Petrol. 44, 679–711.

Gross, A.O.M.S., Droop, G.T.R., Porcher, C.C., Fernandes, L.A.D., 2009. Petrology and

thermobarometry of mafic granulites and migmatites from the Chafalote Metamorphic

Suite: New insights into the Neoproterozoic P-T evolution of the Uruguayan–Sul-Rio-

Grandense shield. Precambrian Res. 170, 157–174.

Hartmann, L.A., Santos, J.O.S., Bossi, J., Campal, N., Schipilov, A., McNaughton, N.J.,

2002. Zircon and titanite U–Pb SHRIMP geochronology of Neoproterozoic felsic

magmatism on the eastern border of the Rio de le Plata Craton, Uruguay. J. South Am.

Earth Sci. 15, 229–236.

Heine, C., Zoethout, J., Müller, R.D., 2013. Kinematics of the South African rift. Sol. Earth 4,

215–253.

_____

Jacobsen, S.B., Wasserburg, G.J., 1980. Sm–Nd isotopic evolution of chondrites. Earth

    Planet. Sci. Lett. 50, 139–155.

Jackson, S.E., Pearson, N.J., Griffin, W.L., Belousova, E.A., 2004. The application of laser

    ablation-inductively coupled plasma-mass spectrometry to in situ U–Pb zircon

    geochronology. Chem. Geol. 211, 47–69.

Janoušek, V., Konopásek, J., Ulrich, S., Erban, V., Tajčmanová, L., Jeřábek, P., 2010.

    Geochemical character and petrogenesis of Pan-African Amspoort suite of the Boundary

    Igneous Complex in the Kaoko Belt (NW Namibia). Gondwana Res. 18, 688–707.

Koester, E., Porcher, C.C., Pimentel, M.M., Fernandes, L.A.D., Vignol-Lelarge, M.L.,

    Oliveira, L.D., Ramos, R.C., 2016. Further evidence of 777 Ma subduction-related

    continental arc magmatism in Eastern Dom Feliciano Belt, southern Brazil: the Chácara

    das Pedras Orthogneiss. J. South Am. Earth Sci. in press, doi:

    0.1016/j.jsames.2015.12.006.

Koester, E., Soliani Jr., E., Leite, J.A.D., Hartmann, L.A., Fernandes, L.A.D., McNaughton,

    N.J., Santos, J.O.S., de Oliveira, L.D., 2001. SHRIMP U–Pb age for the emplacement of

    the Santana Granite and reactivation of the Porto Alegre Suture, southern Brazil. J. South

    Am. Earth Sci. 14, 91–99.

Konopásek, J., Košler, J., Sláma, J., Janoušek, V., 2014. Timing and sources of pre-collisional

    Neoproterozoic sedimentation along the SW margin of the Congo Craton (Kaoko Belt,

    NW Namibia). Gondwana Res. 26, 386–401.

Konopásek, J., Košler, J., Tajčmanová, L., Ulrich, S., Kitt, S.L., 2008. Neoproterozoic

    igneous complex emplaced along major tectonic boundary in the Kaoko Belt (NW

    Namibia): ion probe and LA-ICP-MS dating of magmatic and metamorphic zircons. J.

    Geol. Soc. London 165, 153–165.

_____

Kröner, S., Konopásek, J., Kröner, A., Passchier, C.W., Poller, U., Wingate, M.T.D.,

  Hofmann, K.H., 2004. U–Pb and Pb-Pb zircon ages of metamorphic rocks in the Kaoko

  Belt of Northwestern Namibia: A Palaeo- to Mesoproterozoic basement reworked during

  the Pan-African orogeny. South Afr. J. Geol. 107, 455–476.

Leite, J.A.D., Hartman, L.A., McNaughton, N.J., Chemale Jr., F., 1998. SHRIMP U/Pb zircon

  geochronology of Neoproterozoic juvenile and crustal-reworked terranes in southernmost

  Brazil. Int. Geol. Rev. 40, 688–705.

Lenz, C., Fernandes, L.A.D., McNaughton, N.J., Porcher, C.C., Masquelin, H., 2011. U–Pb

  SHRIMP ages for the Cerro Bori orthogneisses, Dom Feliciano Belt in Uruguay:

  Evidences of a ~800 Ma magmatic and ~650 Ma metamorphic event. Precambrian Res.

  185, 149–163.

Le Pichon, X., Hayes, D.E., 1971. Marginal Offsets, Fracture Zones, and the Early Opening

  of the South Atlantic. J. Geophys. Res. 76, 6283–6293.

Le Roex, A.P., Lanyon, R., 1998. Isotope and trace element geochemistry of Cretaceous

  Damaraland lamprophyres and carbonatites, northwestern Namibia: Evidence for plume–

  lithosphere interactions. J. Petrol. 39, 1117–1146.

Ludwig, K.R., 1998. On the treatment of concordant uranium-lead ages. Geoch. Cosmoch.

  Acta 62, 665–676.

Ludwig, K.R., 2012. Isoplot 3.75. A geochronological toolkit for Microsoft Excel. Berkley

  Geochronology Center Special Publication No. 5.

Lugmair, G.W., Marti, K., 1978. Lunar initial $^{143}$Nd/$^{144}$Nd: Differential evolution of the lunar

  crust and mantle: Earth Planet. Sci. Lett. 39, 349–357.

Martin, A.K., Hartnady, C.J.H., Goodlad, S.W., 1981. A revised fit of South America and

  South Central Africa. Earth Planet. Sci. Lett. 54, 293–305.

_____

Martini, A., Bitencourt, M.F., Nardi, L.V.S., Florisbal, L.M., 2015. An integrated approach to

the late stages of Neoproterozoic post-collisional magmatism from Southern Brazil:

Structural geology, geochemistry and geochronology of the Corre-mar Granite.

Precambrian Res. 261, 25–39.

Michard, A., Gurriet, P., Soudant, M., Albarède, F., 1985. Nd isotopes in French Phanerozoic

shales: External vs. internal aspects of crustal evolution. Geoch. Cosmoch. Acta 49, 601–

610.

Moulin, M., Aslanian, D., Unternehr, P., 2010. A new starting point for the South and

Equatorial Atlantic Ocean. Earth Sci. Rev. 98, 1–37.

Nürnberg, D., Müller, R.D., 1991. The tectonic evolution of the South Atlantic from Late

Jurassic to present. Tectonophysics 191, 27–53.

Ortelius, A., 1596. Thesaurus Geographicus (third edition).

Oyhantçabal, P., Siegesmund, S., Wemmer, K., Passchier, C.W., 2011. The transpressional

connection between Dom Feliciano and Kaoko Belts at 580–550 Ma. Int. J. Earth Sci.

100, 379–390.

Oyhantçabal, P., Siegesmund, S., Wemmer, K., Presnyakov, S., Layer, P., 2009.

Geochronological constraints on the evolution of the southern Dom Feliciano Belt

(Uruguay). J. Geol. Soc. London 166, 1075–1084.

Passarelli, C.R., Basei, M.A.S., Siga Jr., O., Mc Reath, I., Campos Neto, M.C., 2010.

Deformation and geochronology of syntectonic granitoids emplaced in the Major Gercino

Shear Zone, southeastern South America. Gondwana Res. 17, 688–703.

Patchett, P.J., Tatsumoto, M., 1980. Hafnium isotope variations in oceanic basalts: Geophys.

Res. Lett. 7, 1077–1080.

_____

Paton, C., Hellstrom, J., Paul, B., Woodhead, J., Hergt, J., 2011. Iolite: Freeware for the

visualisation and processing of mass spectrometric data. J. Anal. Atom. Spec. 26, 2508–

2518.

Paton, C., Woodhead, J.D., Hellstrom, J.C., Hergt, J.M., Greig, A., Maas, R., 2010. Improved

laser ablation U–Pb zircon geochronology through robust downhole fractionation

correction. Geochem. Geophys. Geosyst. 11, Q0AA06.

Petrus, J.A., Kamber, B.S., 2012. VizualAge: A Novel Approach to Laser Ablation ICP-MS

U–Pb Geochronology Data Reduction. Geostand. Geoanal. Res. 36, 247–270.

Porada, H., 1979. Damara-Ribeira orogeny of the Pan-African-Brasiliano cycle in Namibia

(Southwest Africa) and Brazil as interpreted in terms of continental collision.

Tectonophysics 57, 237–265.

Rabinowitz, P.D., LaBrecque, J., 1979. The Mesozoic South Atlantic Ocean and Evolution of

Its Continental Margins. J. Geophys. Res. 84, 5973–6002.

Remus, M.V.D., Hartmann, L.A., McNaughton, N.J., Groves, D.I., Fletcher, I.R., 2000. The

link between hydrothermal epigenetic copper mineralization and the Caçapava Granite of

the Brasiliano Cycle in southern Brazil. J South Am. Earth Sci. 13, 191–216.

Remus, M.V.D., McNaughton, N.J., Hartmann, L.A., Koppe, J.C., Fletcher, I.R., Groves, D.I.,

Pinto, V.M., 1999. Gold in Neoproterozoic juvenile Bossoroca Volcanic Arc of

southernmost Brazil: isotopic constraints on timing and sources. J. South Am. Earth Sci.

12, 349–366.

Scherer, E., Munker, C., Mezger, K., 2001. Calibration of the lutetium-hafnium clock.

Science 293, 683–687.

Seth, B., Kröner, A., Mezger, K., Nemchin, A.A., Pidgeon, R.T., Okrusch, M., 1998.

Archaean to Neoproterozoic magmatic events in the Kaoko belt of NW Namibia and their

geodynamic significance. Precambrian Res. 92, 341–363.

_____

Sibuet, J.-C., Mascle, J., 1978. Plate Kinematic Implications of Atlantic Equatorial Fracture
Zone Trends. J. Geophys. Res. 83, 3401–3421.

Sláma, J., Košler, J., Condon, D.J., Crowley, J.L., Gerdes, A., Hanchar, J.M., Horstwood,
M.S.A., Morris, G.A., Nasdala, L., Norberg, N., Schaltegger, U., Schoene, B., Tubrett,
M.N., Whitehouse, M.J., 2008. Plešovice zircon - A new natural reference material for
U–Pb and Hf isotopic microanalysis. Chem. Geol. 249, 1–35.

Smith, A.G., Hallam, A., 1970. The fit of the southern continents. Nature 225, 139–144.

Stacey, J.S., Kramers, J.D., 1975. Approximation of terrestrial lead isotope evolution by a
two-stage model. Earth Planet. Sci. Lett. 26, 207–221.

Steiger, R.H., Jaeger, E., 1977. Subcommission on geochronology: Convention on the use of
decay constants in geo- and cosmochronology. Earth Planet. Sci. Lett. 36, 359–362.

Torsvik, T.H., Rousse, S., Labails, C., Smethurst, M.A., 2009. A new scheme for the opening
of the South Atlantic Ocean and the dissection of an Aptian salt basin. Geophys. J. Int.
177, 1315–1333.

Unternehr, P., Curie, D., Olivet, J.L., Goslin, J., Beuzart, P., 1988. South Atlantic fits and
intraplate boundaries in Africa and South America. Tectonophysics 155, 169–179.

Vervoort, J.D., Patchett, P.J., Soderlund, U., Baker, M., 2004. Isotopic composition of Yb and
the determination of Lu concentrations and Lu/Hf ratios by isotope dilution using MC–
ICPMS. Geochem. Geophys. Geosyst. 5, Q11002.

Vink, G.E., 1982. Continental Rifting and the Implications for Plate Tectonic
Reconstructions. J. Geophys. Res. 87, 10667–10688.

Wasserburg, G.J., Jacobsen, S.B., DePaolo, D.J., McCulloch, M.T., Wen, T., 1981. Precise
determination of Sm/Nd ratios, Sm and Nd isotopic abundances in standard solutions.
Geochim. Cosmochim. Acta 45, 2311–2323.

_____

Wegener, A., 1912. Die Entstehung der Kontinente. Dr. A. Petermanns Mitteilungen aus
    Justus Perthes' Geographischer Anstalt 63, 185–195, 253–256, 305–309.

Whitehouse, M.J., Kamber, B.S., 2005. Assigning dates to thin gneissic veins in high-grade
    metamorphic terranes: A cautionary tale from Akilia, southwest Greenland. J. Petrol. 46,
    291–318.

Whitehouse, M.J., Kamber, B.S., Moorbath, S., 1999. Age significance of U–Th–Pb zircon
    data from early Archaean rocks of west Greenland—a reassessment based on combined
    ion-microprobe and imaging studies. Chem. Geol. 160, 201–224.

Wiedenbeck, M., Alle, P., Corfu, F., Griffin, W.L., Meier, M., Oberli, F., Vonquadt, A.,
    Roddick, J.C., Speigel, W., 1995. Three natural zircon standards for U-Th-Pb, Lu-Hf,
    trace element and REE analyses. Geost. Newsletter 19, 1–23.

Wu, F.Y., Yang, Y.H., Xie, L.W., Yang, J.H., Xu, P., 2006. Hf isotopic compositions of the
    standard zircons and baddeleyites used in U–Pb geochronology. Chem. Geol. 234, 105–
    126.

**FIGURE CAPTIONS**

Figure 1. Simplified geological map of the Dom Feliciano and Kaoko belts (modified after

Gross et al., 2009 and Frimmel et al., 2011). The mutual position of Africa and South

America is shown at 140 Ma (see inset), the dot-and-dash line shows the inferred position of

the rift centre after Heine et al. (2013). AFMC–Angra Fria Magmatic Complex.

(Meta)cratonic domains: 1–Congo; 2–Kalahari; 3–Rio de la Plata; 4–Luis Alves. A– Sierra

Ballena-Dorsal Canguçu-Major Gercino shear zone; B–Village-Three Palm shear zone

_____

system. MV–Montevideo; PA–Porto Alegre; FL–Florianópolis; LÜ–Lüderitz; SW–

Swakopmund.

Figure 2. Detailed geological map of the Angra Fria Magmatic Complex in the area of the Old

Cape Fria Radio Station with the location of the samples used for this study.

Figure 3. Photographs of the AFMC rocks and their field relationships. a) Intrusive

relationships between the older (dark), deformed magmatic suite and undeformed younger

(pink) granitoids. b) Granitic orthogneiss sample NJ-57. c) Hornblende gabbro sample NJ-58.

d) Dioritic dyke (sample NJ-05) intruding migmatitic gneisses of the Coastal Terrane.

Figure 4. U–Pb concordia plots for samples dated by LA–ICP–MS with cathodoluminescence

images of typical zircons. Error ellipses are plotted at 2σ level. MSWD – mean square of

weighted deviates. Grey ellipses show dates not involved in the age calculation.

Figure 5. Comparison of initial (i) $^{87}Sr/^{86}Sr$ and εNd values for the Angra Fria Magmatic

Complex granitoids with the data of Florisbal et al. (2012b),  Florisbal et al. (2012c) and

Chemale et al. (2012) for the Florianópolis Batholith granitoids and granitoids intruding the

foreland northwest of this batholith.

Figure 6. U–Pb concordia plots for samples dated by SIMS with cathodoluminescence image

of typical zircon in sample NK-42. Error ellipses are plotted at 2σ level. MSWD – mean

square of weighted deviates.

Figure 7. Summary of zircon protolith ages (whiskers show published errors) for the Florianópolis, Pelotas and Aiguá batholiths and intrusions into the neighboring foreland domain (Babinski et al., 1997; Leite et al., 1998; Remus et al., 1999; 2000; Koester et al., 2001; da Silva et al., 1999; 2005; Hartmann et al., 2002; Gaucher et al., 2008; Oyhantçabal et al., 2009; Passarelli et al., 2010; Basei et al., 2011; Chemale et al., 2012; Florisbal et al., 2012a; Martini et al., 2015), and for the intrusive rocks of the Costal Terrane in the Kaoko Belt (Seth et al., 1998; Kröner et al., 2004; Konopásek et al., 2008). Grey stripes show inferred time interval for the emplacement of the older and younger AFMC suite.

**Table**

Table 1: Analytical results of the whole rock Sr-Nd isotopic analysis.

| Sample | age (i) (Ma) | Rb (ppm) | Sr (ppm) | $\frac{^{87}Rb}{^{86}Sr}$ | $\frac{^{87}Sr}{^{86}Sr}$ | $\frac{^{87}Sr}{^{86}Sr_{(i)}}$ | $2\sigma$ | Sm (ppm) |
|---|---|---|---|---|---|---|---|---|
| NJ-57 | 626 | 121.3 | 270.8 | 1.2969 | 0.719309 | 0.707711 | 0.000009 | 2.6 |
| NJ-59 | 620 | 74.7 | 473.5 | 0.4566 | 0.711879 | 0.707841 | 0.000009 | 6.7 |
| NJ-58 | 622 | 35.6 | 112.5 | 0.9160 | 0.715108 | 0.706982 | 0.000009 | 9.7 |
| NJ-62 | 574 | 243.9 | 65.2 | 10.9266 | 0.799878 | 0.710453 | 0.000008 | 5.7 |
| NJ-05 | 584 | 50.9 | 351.1 | 0.4194 | 0.715243 | 0.711750 | 0.000009 | 7.0 |
| NK-42 | 586 | 131.6 | 206.9 | 1.8437 | 0.728083 | 0.712677 | 0.000009 | 6.0 |

**Figure1**
**Click here to download high resolution image**
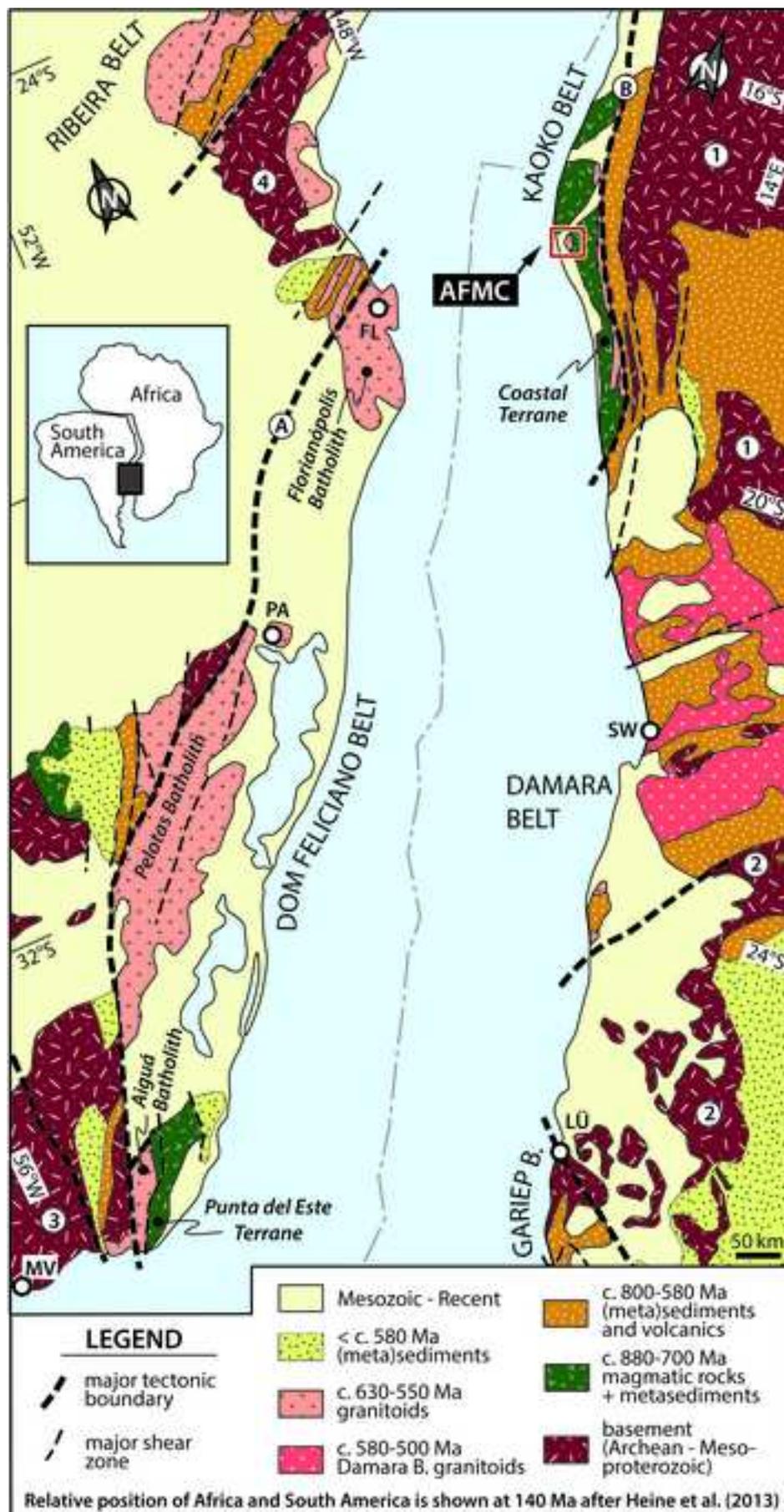
Konopásek et al. - Fig. 1 - **single column width**
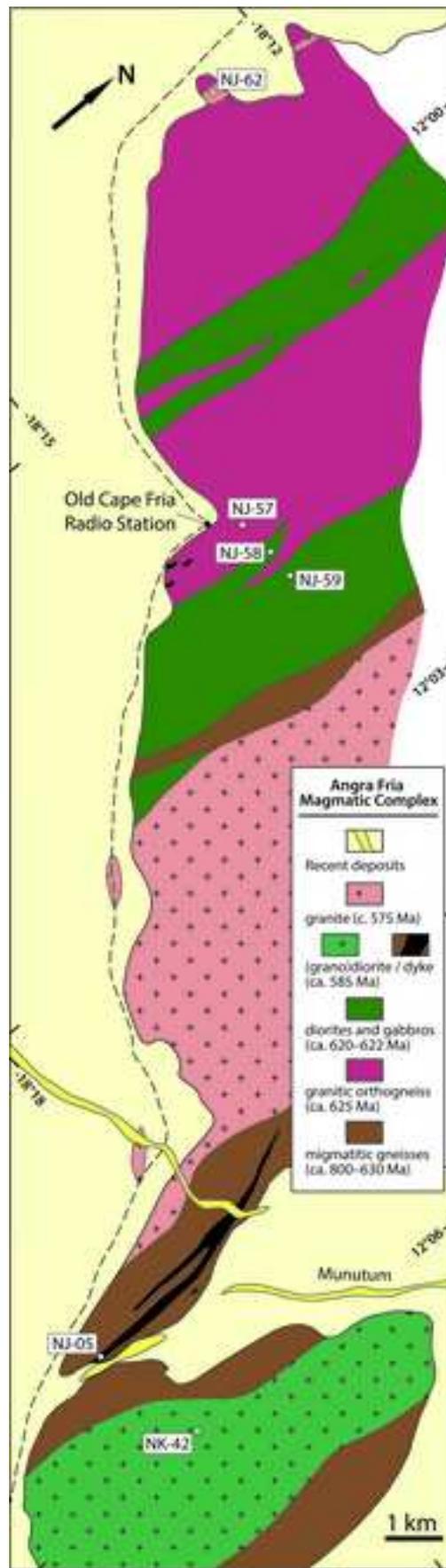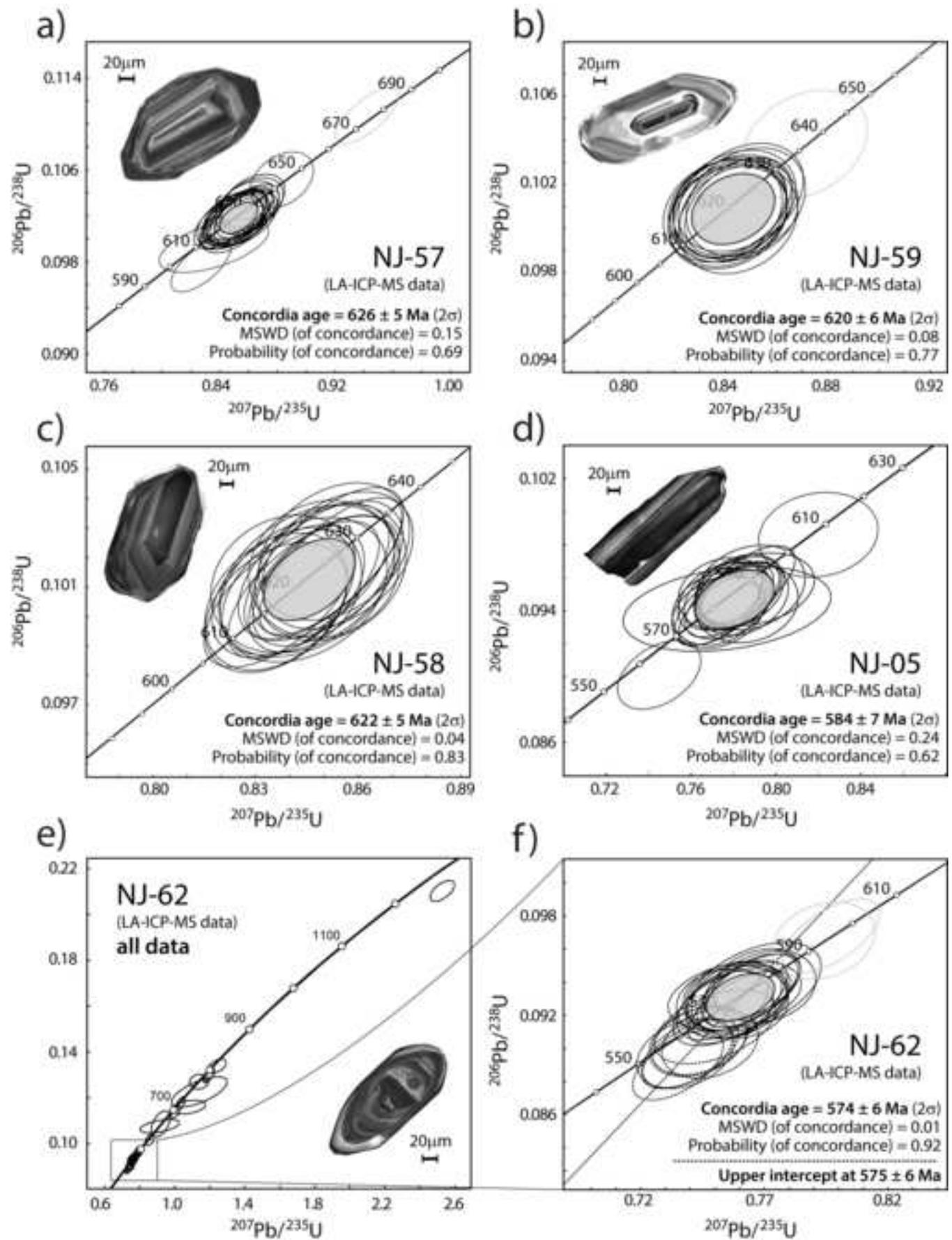
Konopásek et al. - Fig. 2
single column width

**Figure3**
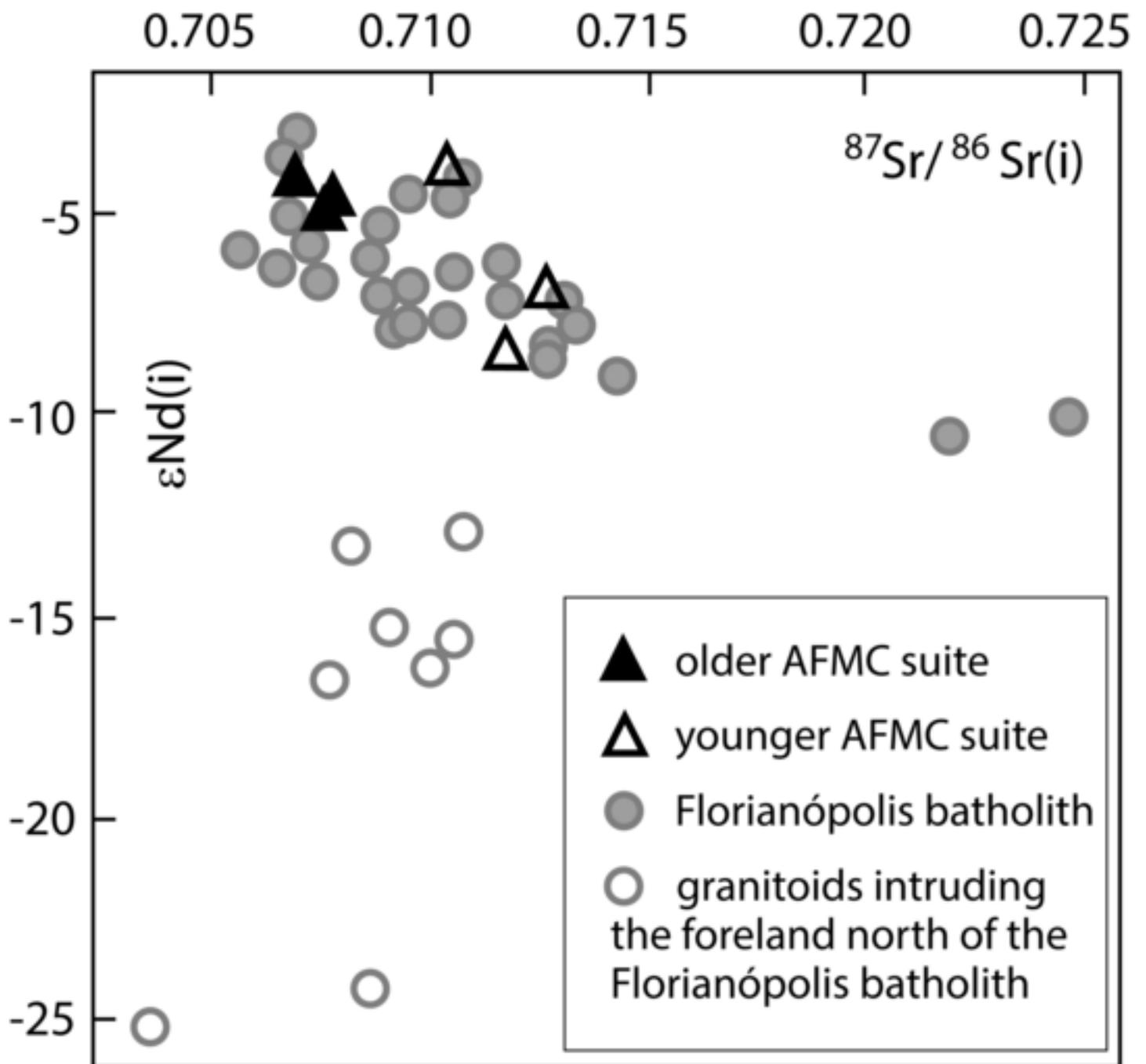**Click here to download high resolution image**
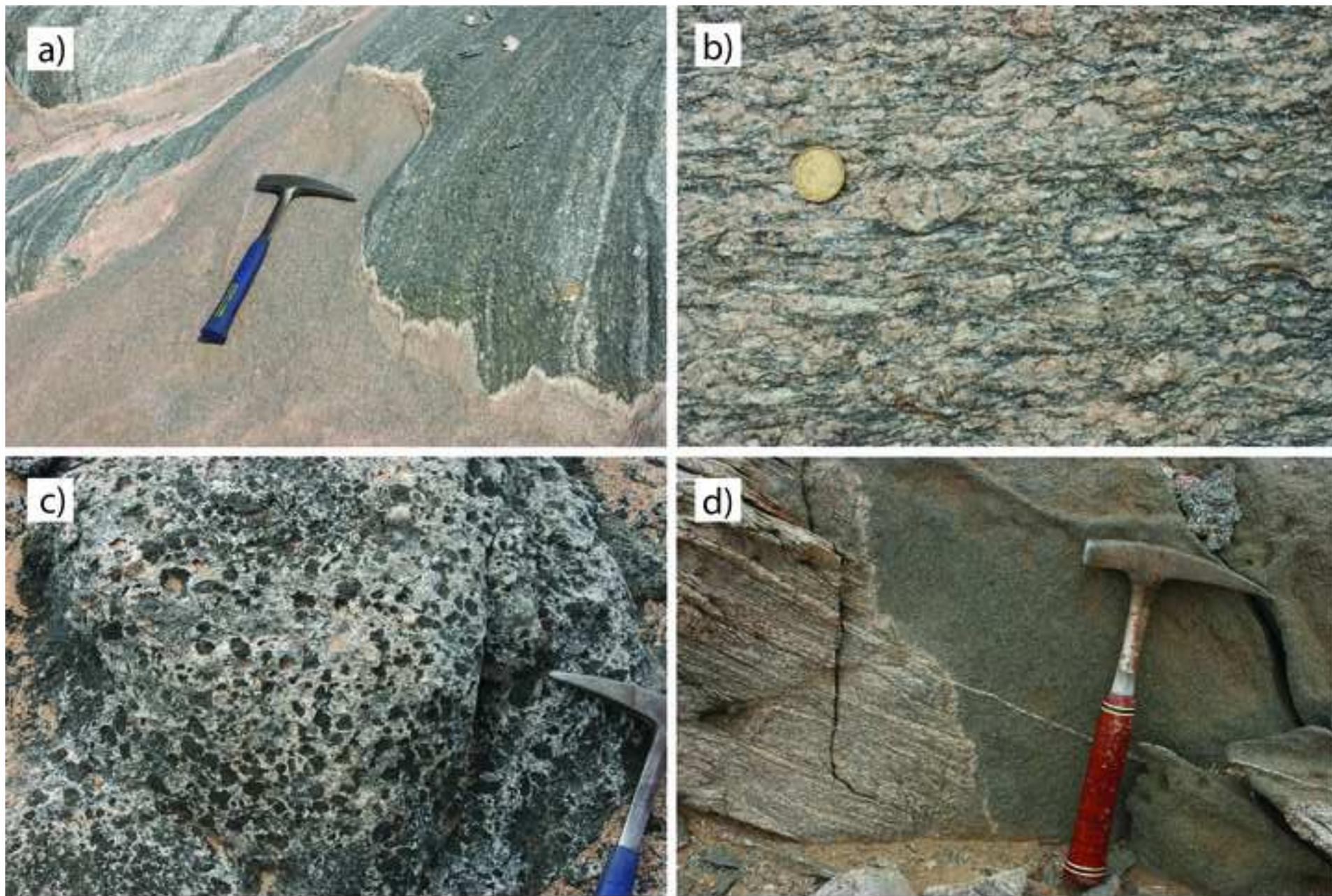
Konopásek et al. - Fig. 3 - **double column width**
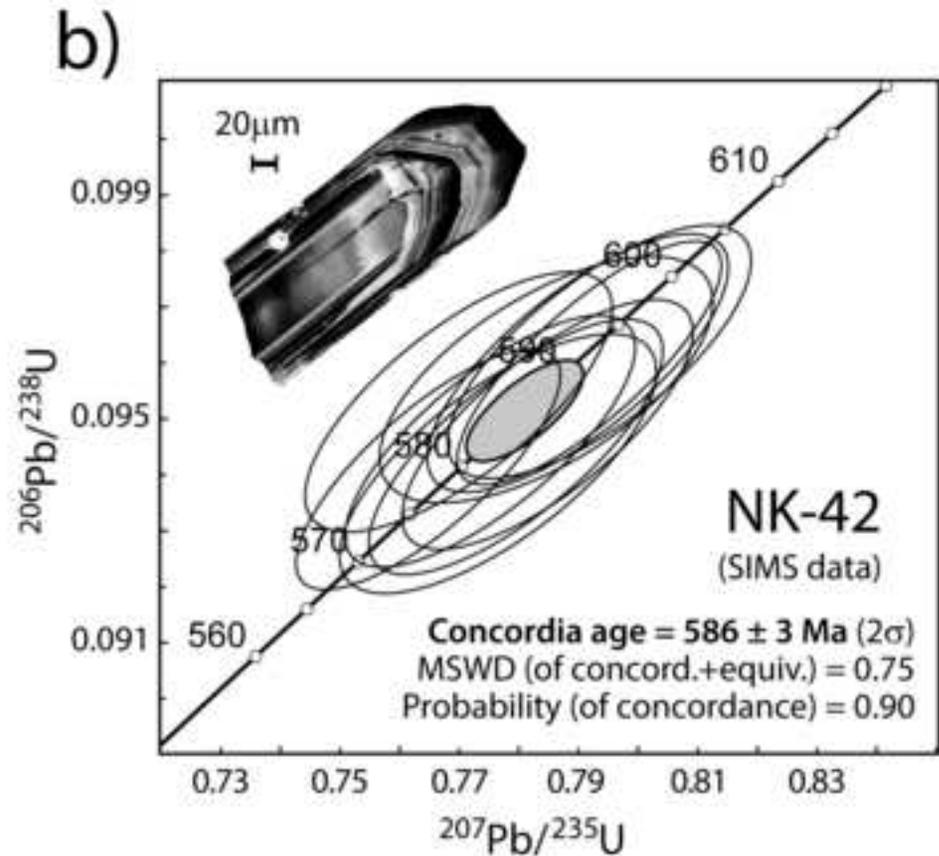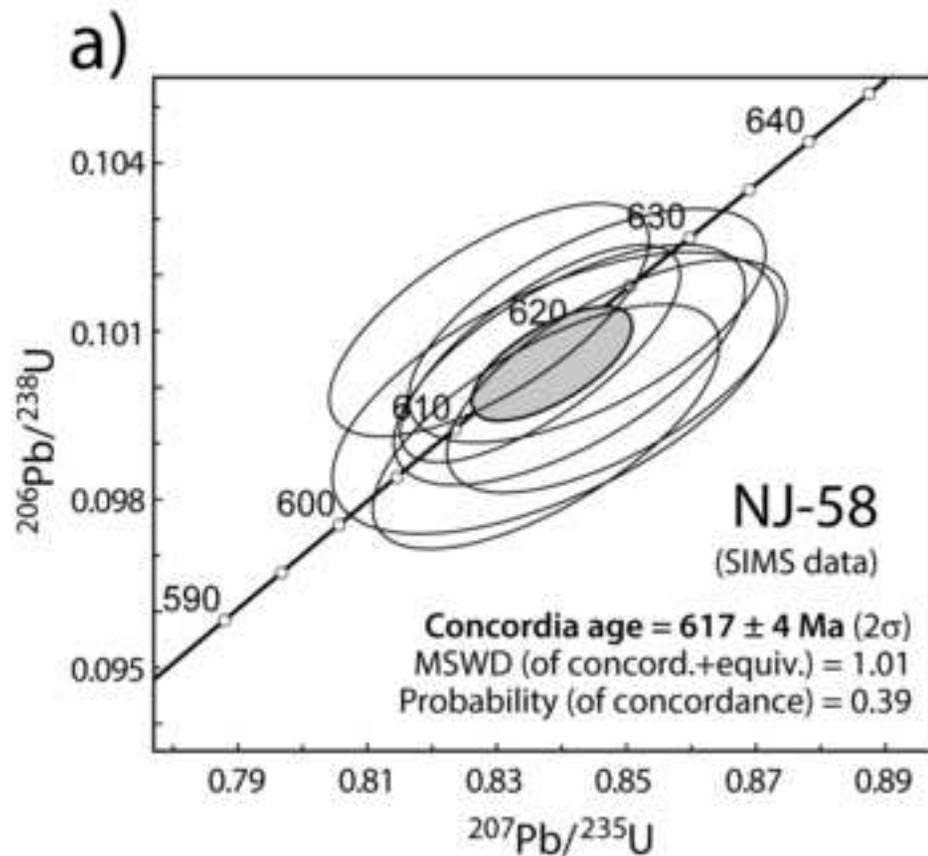
**Figure4**
**Click here to download high resolution image**

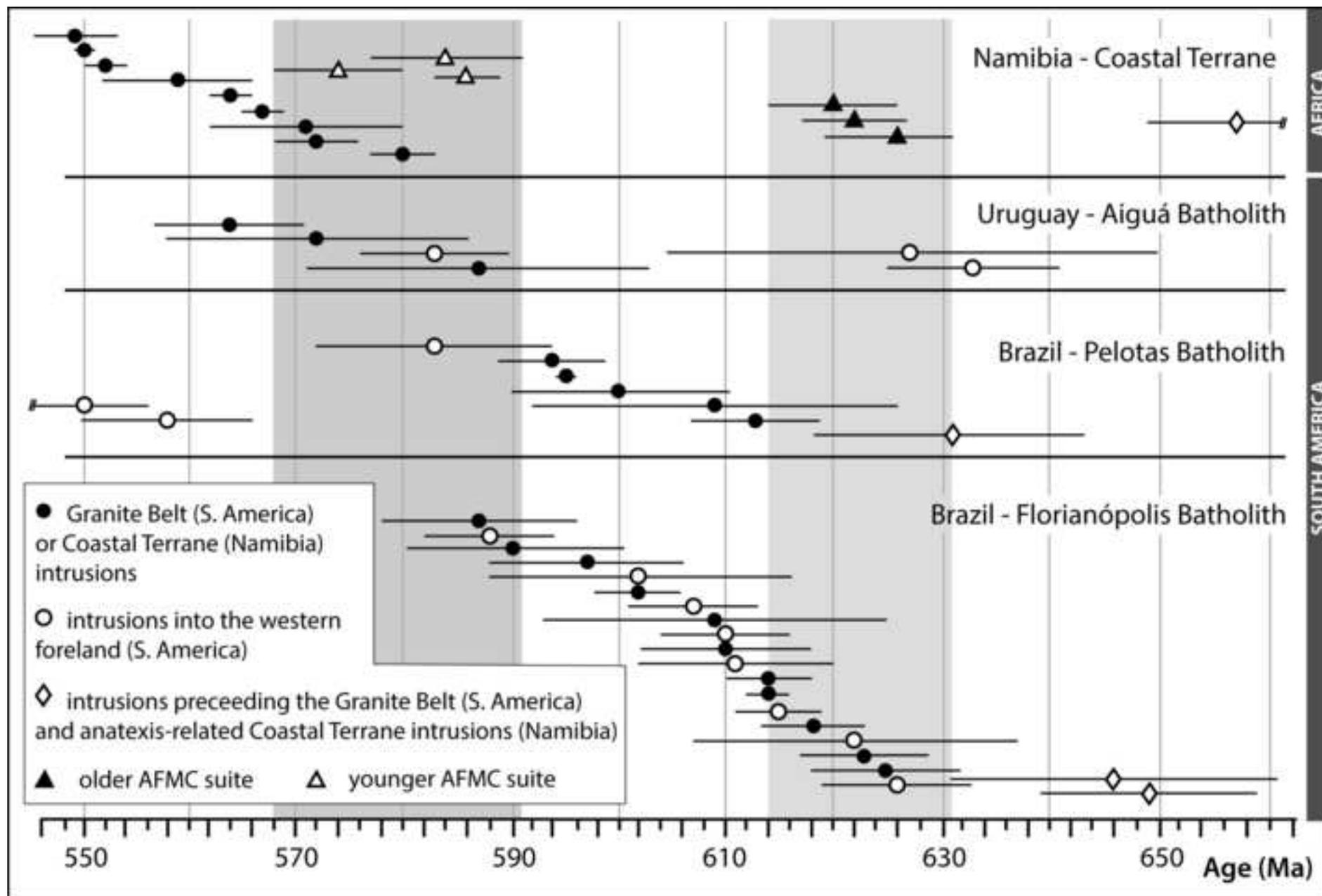Konopásek et al. - Fig. 4 - **1.5 or 2-column width**

Konopasek et al. - Fig. 5
single column width

Konopásek et al. - Fig. 6 - **1.5 or 2-column width**

**Figure7**
**Click here to download high resolution image**

Konopásek et al. - Fig. 7 - **double column width**